Bioactive Materials 27 (2023) 362–376

Contents lists available at ScienceDirect

Bioactive Materials

journal homepage: www.keaipublishing.com/en/journals/bioactive-materials

A novel bioartificial pancreas fabricated via islets microencapsulation in anti-adhesive core-shell microgels and macroencapsulation in a hydrogel scaffold prevascularized in vivo

Haofei Li [a,b,c,1], Yulian Shang [a,b,d,1], Qi Feng [a,b,c,e], Yang Liu [a,b,c], Junlin Chen [a,b,c], Hua Dong [a,b,c,e,*]

[a] School of Materials Science and Engineering, South China University of Technology, Guangzhou, 510006, China
[b] National Engineering Research Center for Tissue Restoration and Reconstruction (NERC-TRR), Guangzhou, 510006, China
[c] Key Laboratory of Biomedical Materials and Engineering of the Ministry of Education, South China University of Technology, Guangzhou, 510006, China
[d] School of Biomedical Science and Engineering, South China University of Technology, Guangzhou, 510006, China
[e] Guangdong Province Key Laboratory of Biomedical Engineering, South China University of Technology, Guangzhou, 510641, China

ARTICLE INFO

Keywords:
Type 1 diabetes
Bioartificial pancreas
Islet encapsulation
Core-shell microgel
Prevascularized scaffold

ABSTRACT

Islets transplantation is a promising treatment for type 1 diabetes mellitus. However, severe host immune rejection and poor oxygen/nutrients supply due to the lack of surrounding capillary network often lead to transplantation failure. Herein, a novel bioartificial pancreas is constructed via islets microencapsulation in core-shell microgels and macroencapsulation in a hydrogel scaffold prevascularized in vivo. Specifically, a hydrogel scaffold containing methacrylated gelatin (GelMA), methacrylated heparin (HepMA) and vascular endothelial growth factor (VEGF) is fabricated, which can delivery VEGF in a sustained style and thus induce subcutaneous angiogenesis. In addition, islets-laden core-shell microgels using methacrylated hyaluronic acid (HAMA) as microgel core and poly(ethylene glycol) diacrylate (PEGDA)/carboxybetaine methacrylate (CBMA) as shell layer are prepared, which provide a favorable microenvironment for islets and simultaneously the inhibition of host immune rejection via anti-adhesion of proteins and immunocytes. As a result of the synergistic effect between anti-adhesive core-shell microgels and prevascularized hydrogel scaffold, the bioartificial pancreas can reverse the blood glucose levels of diabetic mice from hyperglycemia to normoglycemia for at least 90 days. We believe this bioartificial pancreas and relevant fabrication method provide a new strategy to treat type 1 diabetes, and also has broad potential applications in other cell therapies.

1. Introduction

Type 1 diabetes mellitus (T1DM) is an autoimmune disease caused by the destruction of insulin-producing β cells in pancreas, resulting in absolute insulin deficiency [1–3]. In addition to persistent hyperglycemia and disorder of the endocrine system, diabetic patients often suffer from a variety of complications, such as cardiomyopathy, retinopathy, nephropathy, neuropathy, etc [4,5]. Although exogenous insulin injection can relieve these symptoms to some extent, it is still unable to regulate blood glucose levels (BGLs) in a real-time dynamic manner like natural pancreas [6]. Besides, frequent blood glucose monitoring and insulin injection also put a considerable mental and financial burden on patients with T1DM, as well as inconvenience to their daily life [7].

The most promising solution to this dilemma is islets transplantation that can reconstruct the endogenous insulin secretion to achieve insulin independence [8]. Despite of the well-known merits, clinical trials of islets transplantation are not prevalent, due to the vigorous host immune rejection and resultant massive islets apoptosis after transplantation [9,10]. To alleviate the host immune rejection after islets transplantation, long-term administration of immune-suppressants is required, which undermines body resistivity to other diseases [11,12]. Another alternative to immunosuppressant is islets encapsulation in biocompatible

Peer review under responsibility of KeAi Communications Co., Ltd.
* Corresponding author. School of Materials Science and Engineering, South China University of Technology, Guangzhou, 510006, China.
E-mail address: donghua@scut.edu.cn (H. Dong).
[1] These authors contributed equally to this work.

https://doi.org/10.1016/j.bioactmat.2023.04.011
Received 13 November 2022; Received in revised form 30 March 2023; Accepted 11 April 2023

polymer-based materials that separate islets from immunocytes but simultaneously allow the entry and exit of nutrients, metabolites and insulin [13–16]. Depending on the dimension of encapsulation materials, islets encapsulation strategies can be classified into macroencapsulation, microencapsulation and nanoencapsulation [17–25]. Generally speaking, these three encapsulation strategies have their own pros and cons. For example, macroencapsulation is beneficial for the retrieve of transplanted islets, but the large device size increases the delivery distance of oxygen and nutrients [26]. Islets encapsulation in microgels or microcapsules offers favorable microenvironment and also enables minimally invasive treatment. However, it is hard to locate the grafts especially when transplanting them into the sites such as hepatic portal veins [27,28]. Nanoencapsulation induces the minimum thrombus effect, but the instability of nanolayer coated on the islets surface often leads to the reactivation of host immune rejection. As a consequence, there is still an urgent need to develop a new strategy that can make full use of the advantages and avoid the disadvantages of these encapsulation methods.

Except for host immune rejection, the complicated surgical procedures of traditional islets transplantation into either hepatic portal vein, or peritoneum, or epididymal fat pad and the difficulty in retrieving these grafts, also increase the operation cost and risk of patient's postoperative recovery [29–31]. Comparatively, subcutaneous islets transplantation is very appealing because of the abundant sites available for transplantation, the least invasion to the body and the ease to monitor, retrieve and update the grafts [32–34]. Unfortunately, insufficient blood vessel network inside skin tissue cannot meet the high O_2 and nutrient requirement for islets survival and insulin secretion [35–37]. Prevascularization of the potential subcutaneous transplantation site, prior to islets transplantation, may possibly address this problem [38–40]. Even with the mature angiogenesis approaches by delivering angiogenic factors or endothelial cells, it is still a challenge to accelerate the angiogenesis process in transplantation site while still reserve enough space for islets.

In this paper, we report a novel bioartificial pancreas for subcutaneous transplantation to treat type 1 diabetes. In particular, herein we propose a new strategy to construct bioartificial pancreas via islets microencapsulation in anti-adhesive core-shell microgels and subsequently macroencapsulation in prevascularized scaffold (Scheme 1). Specifically, a hydrogel tube scaffold with sustained-release of angiogenic factor is subcutaneously implanted, which can recruit surrounding endothelial cells to form blood capillaries. In the meantime, islets-laden core-shell microgels are prepared via droplet-based microfluidics and interfacial photopolymerization. Thereafter, these microgels are injected into the lumen of prevascularized hydrogel tube scaffold. The abundant vascular network in prevascularized scaffold provides quick O_2 and nutrients supply, whilst the core of core-shell microgels offers islets a favorable microenvironment and the zwitterionic shell of core-shell microgels inhibits the host immune rejection via anti-adhesion of protein and immunocyte. The bioartificial pancreas based on core-shell microgels and macroscale prevascularized scaffold exploits the merits of both microencapsulation and macroencapsulation, and their synergism improves remarkably the islets survival and their insulin-secretion function in vivo. The bioartificial pancreas and relevant fabrication strategy described in this work give a new insight for other cell therapies.

2. Materials and methods

2.1. Materials and reagents

Gelatin, hyaluronic acid, poly(ethylene glycol) diacrylate (PEGDA, 1000 Da), agarose, methacrylic anhydride, 5-aminofluorescein, dimethyl sulfoxide (DMSO), 1-ethyl-3-(3- dimethylaminopropyl-carbodiimide) hydrochloride (EDC), N-hydroxysuccinimide (NHS), lithium phenyl-2,4,6-trimethylbenzoylphosphinate (LAP), 3, 3′-diaminobenzidine (DAB) and histopaque-1077 were purchased from Sigma (USA). Streptozotocin (STZ), heparin sodium, crystal violet,

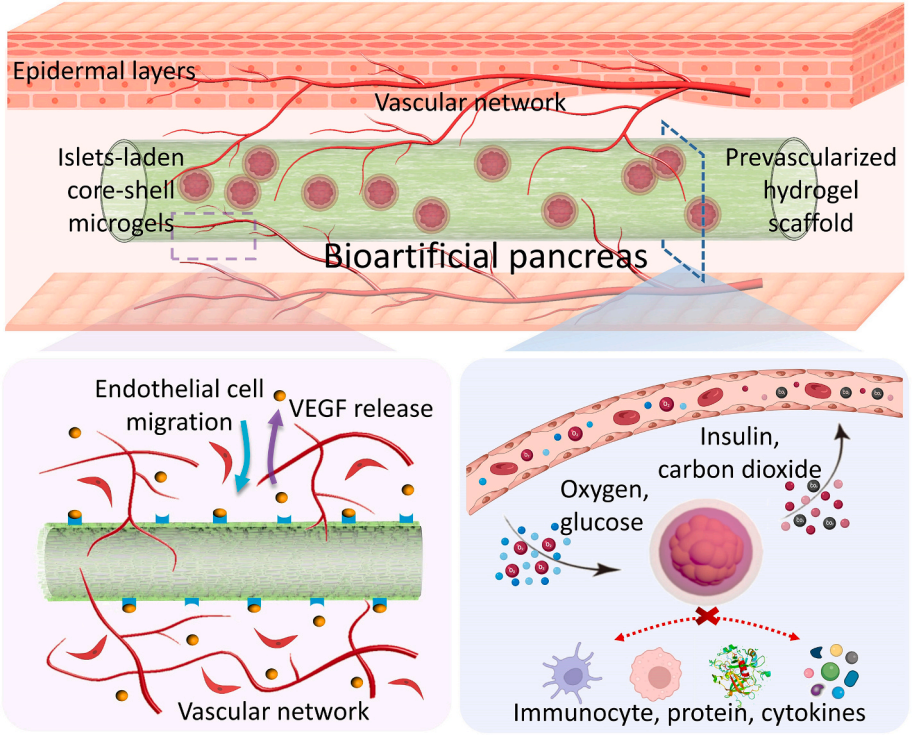

Scheme 1. Schematic illustration on bioartificial pancreas transplanted subcutaneously for type 1 diabetes treatment, where islets are microencapsulated in anti-adhesive core-shell microgels and macroencapsulated in a prevascularized hydrogel scaffold. Vascular network in prevascularized hydrogel scaffold supplies nutrients and oxygen to islets, whilst core-shell microgels provide immune-protection and favorable microenvironment for islets.

pentobarbital sodium, dimethylaminoethyl methacrylate (DMAEMA), 4-methoxyphenol, acrylic acid, triethylamine and paraformaldehyde were obtained from Aladdin (Shanghai, China). Collagenase P was provided by Roche Biochemicals (Basel, Switzerland). Isoflurane was bought from RWD Life Science Co., Ltd. (Shenzhen, China). Fluorescent polystyrene (PS) microbeads were purchased from BaseLine Company (Tianjin, China). Fluorescein isothiocyanate-labelled bovine serum albumin (FITC-BSA) and lipopolysaccharide (LPS) were obtained from Solarbio Science & Technology Co., Ltd. (Beijing, China). PDMS (Sylgard 184) and negative resist (NR21-20000P) were bought from Dow Corning Company and Futurrex Inc. (USA) respectively. Fluorinated oil (HFE-7500) was purchased from 3 M (USA) and surfactant (Pico-SurfTM) was purchased from Dolomite Microfluidics (USA). All cell culture reagents and biological assays, including fetal bovine serum (FBS), penicillin/streptomycin (P/S) and Hanks' balanced salt solution (HBSS) were obtained from Beyotime Biotechnology (Shanghai, China) unless otherwise noted. All reagents were of analytical grade and used as received without further purification.

2.2. Preparation and characterization of prevascularized scaffold

2.2.1. Synthesis of methacrylated gelatin (GelMA)

10 g of gelatin was dissolved in 100 mL of PBS under stirring, then 10 mL of methacrylic anhydride was dropwise added into the solution and the reaction was allowed to perform at 50 °C for 3 h. Thereafter, the solution was diluted to 500 mL with PBS to terminate the reaction. Finally, the solution was dialyzed for 7 d and freeze-dried to obtain GelMA.

2.2.2. Synthesis of methacrylated heparin (HepMA)

0.5 g of heparin sodium was dissolved in PBS to form 1 wt% of heparin solution, and then 17.45 mmol of methacrylic anhydride was added dropwise. The reaction was carried out at room temperature for 24 h. During this period, the pH value of the solution was monitored by a pH meter, and sodium hydroxide solution (1 M) was dropwise added to keep the pH of the solution at 8 consistently. Finally, the aqueous solution was dialyzed in deionized water and lyophilized to obtain the resultant HepMA.

2.2.3. Preparation of scaffold for prevascularization

GelMA/HepMA hydrogel precursor solution were first prepared by dissolving 10 wt% of GelMA, 2.5 wt% of HepMA and 0.2 wt% of LAP in PBS, then a biomedical silicon tube (inner diameter: 1.5 mm; outer diameter: 3.0 mm; length: 20.0 mm) was soaked into the solution and ice water was injected into the tube through a syringe. After GelMA/HepMA hydrogel was formed on the silicone tube surface, the tube was irradiated under a hand-held blue light lamp (450 nm) for 2 min. Finally, the tube was soaked in 500 ng mL^{-1} of vascular endothlial growth factor (VEGF) solution at 4 °C overnight to obtain the scaffold for prevascularization. The amounts of immobilized VEGF in the hydrogel scaffolds were quantified by measuring the decrease of VEGF content in immobilization solution by ELISA kit (Jiangsu Jingmei Biological Technology Co., Ltd, China), which were 115.4 ± 5.1, 139.7 ± 8.9, 128.8 ± 5.1 and 156.3 ± 7.6 ng for GelMA/VEGF, GelMA/Heparin2.5/VEGF, GelMA/HepMA2.5/VEGF and GelMA/HepMA5.0/VEGF scaffolds, respectively.

2.2.4. VEGF release behavior

The hydrogel scaffolds were immersed in 2 mL of DPBS supplemented with 0.1% of BSA and maintained at 37 °C with gentle shaking for up to 15 d. The DPBS was collected and replaced with fresh one at predetermined time. The amount of released VEGF was analyzed using ELISA assay.

2.2.5. HUVEC viability and proliferation

The GelMA/HepMA/VEGF hydrogels were transferred into a 24-well culture plate. Then human umbilical vein endothelial cells (HUVECs) were seeded onto the hydrogel surfaces at 100,000 cells per well, and cultured in endothelial medium supplemented with 10% of FBS and 1% of P/S in a CO_2 incubator at 37 °C. Cell viability was assessed by live/dead staining, and the cell proliferation was measured via CCK-8 assay after 1, 3 and 5 d of culture.

2.2.6. HUVEC migration assay

HUVEC migration was evaluated through Boyden chamber assay. HUVECs (1×10^5 mL^{-1}) were seeded upon the filter membrane of 24-well Transwell insert (8 μm pore, Corning) and immersed in endothelial medium. Then GelMA/HepMA/VEGF hydrogel was added into the bottom of the lower chamber in a 24-well plate. After 12 h, HUVECs migrated down to the hydrogels were fixated with 4% of paraformaldehyde, stained with 0.1% (w/v) of crystal violet and imaged with a microscope. The number of migrated HUVECs was quantified with Image J software.

2.2.7. Scaffold implantation

Male C57BL/6J mice (Hunan SJA Laboratory Animal Co., Ltd., China) were anesthetized by intraperitoneal injection of pentobarbital sodium (30 mg kg^{-1} body weight), then their dorsums were shaved and wiped with betadine. An incision was made on the central dorsal surface with scalpel and scaffold was implanted. After skin closure, post-operation care was taken to ensure the recovery of the mice. The surgical procedures were conducted under sterile conditions. All animal procedures were performed in accordance with the Guidelines for Care and Use of Laboratory Animals of South China University of Technology and approved by the Animal Ethics Committee of South China University of Technology. (Approval NO. 2019002).

2.2.8. Histological analysis

The mice were euthanized via CO_2 asphyxiation. The implants with surrounding tissues were collected, fixed in 4% of paraformaldehyde solution, dehydrated, embedded in paraffin, sectioned and stained with hematoxylin and eosin (H&E) which labelled the nuclei in blue and the cell cytoplasm in pink, respectively. For immunohistochemical staining of CD31, the sections were deparaffinized in xylene, rehydrated in a graded series of ethanol solutions, treated with 3% (v/v) of hydrogen peroxide for 20 min to eliminate the activity of endogenous peroxidase at room temperature, steamed in 0.01 M of sodium citrate buffer (pH 6.0) at 90–100 °C for antigen retrieval, blocked with 1 wt% of BSA for 30 min. The sections were then incubated successively with primary antibody of CD31 (1:1000 dilution, Abcam, England) at 4 °C overnight, secondary antibody (biotin conjugated goat anti-mouse IgG) at 37 °C for 30 min, and streptavidin biotin complex (SABC) for 30 min. The sample was visualized using DAB, re-stained with hematoxylin and observed microscopically.

2.3. Preparation and characterization of core-shell microgels

2.3.1. Synthesis of methacrylated hyaluronic acid (HAMA)

2 g of hyaluronic acid was dissolved in 200 mL of deionized water, followed by dropping methacrylic anhydride into the solution at the ratio of 1% (v/v) under ice water bath. The mixture was then stirred at room temperature for 24 h, while keeping the pH of the solution at 8.0. The reaction solution was dialyzed in deionized water for 7 d to remove the excessive methacrylic anhydride. Finally, the reaction product HAMA was obtained by freeze-drying and stored in a constant temperature drying cabinet.

2.3.2. Synthesis of aminofluorescein functionalized HAMA (HAMA-AF)

0.5 g of HAMA was dissolved in 100 mL of deionized water, then 0.3 mmol of EDC and NHS were added into the solution and incubated for 30 min. Subsequently, 8 mg of 5-aminofluorescein dissolved in 10 mL of DMSO was dripped, and the mixture was stirred at room temperature for

24 h in dark. The resultant solution was dialyzed in deionized water and the HAMA-AF was obtained by freeze-drying.

2.3.3. Synthesis of carboxybetaine methacrylate (CBMA)

CBMA monomer was synthesized according to the previously reported procedure [41]. Briefly, 28 mL of DMAEMA and 0.4 g of 4-methoxyphenol were mixed completely under stirring in ice bath. 34 mL of acrylic acid was then added into the mixture at the speed of 1 mL min^{-1}, and stirred for 24 h at room temperature. If the stirring was difficult during this period, 10–20 mL of acetone was added to dilute the reaction solution. Thereafter, the resulting mixture was diluted again with 50 mL of acetone, then excessive acrylic acid was neutralized by 50 mL of triethylamine and the reaction was terminated. Finally, CBMA was precipitated from the solution after adding 100 mL of acetone and washed with 100 mL of acetone for 3–5 times. The precipitation was collected and dried under reduced pressure to obtain the final CBMA monomer product.

2.3.4. Fabrication of microfluidic devices

Droplet-based microfluidic devices were fabricated according to our previous work [42]. Specifically, negative resist was first spin-coated on a clean silicon wafer, and baked at 80 °C for 10 min and 150 °C for 5 min. The resist was then exposed to UV light through a photo-mask and developed in developer solution. The mixture of PDMS base and curing agent (10:1 w/w) was poured onto the silicon wafer, degassed by a vacuum oven and cured on a hotplate at 80 °C for 3 h. The PDMS replica was subsequently peeled off and sealed to glass slide via plasma treatment.

2.3.5. Microfluidic generation of microgels

An appropriate amount of the GelMA or HAMA was first dissolved in PBS, then 0.2 wt% of photoinitiator (LAP) was added into the solution and homogenized by magnetic stirring. The obtained hydrogel precursor solution was injected into microfluidic devices as aqueous phase, which was cut into uniform droplets under the shear force of fluorinated oil containing 0.2 wt% of surfactant. The flow rates of the aqueous phase and oil phase were set as 0.6 and 6 mL h^{-1}, respectively. The collected droplets were converted into microgels after exposing to blue light for 2 min. The solidified microgels were demulsified by replacing fluorinated oil with 20% (v/v) of perfluorooctanol solution, and redistributed into aqueous media for future use.

2.3.6. Preparation of core-shell microgels

Microgels were immersed in 0.2 wt% of LAP for 3 min, rinsed by PBS for 2–3 times quickly and then transferred to the hydrogel precursor solution. After predeterminate time, blue light irradiation was performed to prepare core-shell microgels. The resultant core-shell microgels were observed with a microscope and their size was measured using the Image J software.

2.3.7. Protein adsorption tests

The microgels were incubated in 0.1 mg mL^{-1} of FITC-BSA solutions for 60 min, and washed with PBS for three times to remove the loosely adsorbed proteins on the microgel surface. The adsorbed proteins were visualized by an inverted fluorescence microscope (Axio Observer 7, Zeiss, Germany) and normalized by the relative fluorescent intensity. The test was conducted in triplicate and average values were recorded.

2.3.8. Cell adhesion assay

3% of agarose solution was added into 24-well tissue culture polystyrene (TCPS) plate and the bottom surface of the wells was covered after agarose solidification. Then RAW276.4 macrophages and microgels were added into wells and co-incubated in DMEM medium with 10% of FBS and 1% P/S at 37 °C under 5% of CO_2 for 24 h, and the concentrations of cells and microgels were 400,000/well and 5% (v/v), respectively. Macrophages adhered to the surface of the microgels were stained using calcein AM/ethidium homodimer live/dead assay (Life Technologies, NY, USA), while the free cells were separated through cell strainer. Digitized images were picked with an inverted fluorescence microscope, and the adhesive cells were counted by Image J software.

2.3.9. Zeta potential measurement

The ζ-potential of microgels was measured using Zetasizer Nano ZS (Malvern, U.K.). The value was recorded as the mean of five trials.

2.4. Physical characterization of hydrogels

2.4.1. Preparation of PEGDA/CMBA hydrogel

PEGDA/CMBA hydrogel was prepared by photo-initiated radical copolymerization. Briefly, PEGDA and CMBA was first dissolved in PBS, then 0.2 wt% of LAP was added in the solution and stirred for 10 min. Subsequently, the as-formed homogeneous solution was injected into mold and exposed to blue light for 2 min. The concentration of PEGDA was fixed at 15 wt%, and the CMBA concentration changed accordingly. The obtained PEGDA/CMBA hydrogels were labelled as P/C(x), where x represented the CMBA concentration (wt%).

2.4.2. Swelling behavior of hydrogels

The swelling capacity of the hydrogels was studied by a general gravimetric method. Freshly prepared hydrogel disks (diameter: 13.0 mm, height: 3.0 mm) were weighed to record their initial weights, and then immersed in PBS at 37 °C until swelling equilibrium. Afterward, the fully swollen hydrogel samples were taken out, and weighed after removing excessive liquid on the surface. The swelling ratio (SR) of the hydrogels was defined as: $SR = (W_S–W_0)/W_0 \times 100\%$, where W_S and W_0 were the swollen and initial weights of each sample, respectively. The assay was repeated three times.

2.4.3. Porosity evaluation

The porosity of the hydrogel was determined by the liquid displacement method [43]. Briefly, freeze-dried hydrogel disks (diameter: 13.0 mm, height: 3.0 mm) were immersed in acetone and placed in vacuum to remove the bubble inside the samples. Then the samples were drawn out from acetone and the weight was recorded quickly after the excess solvent on the surface was gently blotted. The porosity (P) was calculated as follows: $P = (W_2–W_1)/\rho V \times 100\%$, where W_1, W_2 and V were dry weight, wet weight and volume of the samples, ρ was the density of acetone.

2.4.4. Mechanical characterization of hydrogels

Compression tests were performed on a universal testing machine (5967, Instron, USA) to measure the mechanical properties of the hydrogels. Hydrogel cylinders (diameter: 4.7 mm, height: 5.0 mm) were compressed at a constant rate of 3 mm min^{-1} and the values of stress and strain were recorded. The compression modules were calculated from the slope of the linear region of the stress-strain curves. At least three samples were tested for each hydrogel.

2.5. Preparation and in vitro characterization of islets-laden core-shell microgels

2.5.1. Islets isolation and purification

Islets were isolated from male Sprague-Dawley (SD) rats (Hunan SJA Laboratory Animal Co., Ltd., China). In brief, the rat was first anesthetized with isoflurane. Then, the bile duct was cannulated with a 30 G needle and the pancreas was perfused with 6–8 mL of Hank's balanced salt solution containing 0.5 mg mL^{-1} of cold collagenase P, allowing the digestion of the pancreas at 37 °C for 20–25 min. Then 20 mL of HBSS buffer solution with 10% of FBS was added to terminate digestion. The digested pancreases were then purified with Histopaque-1077/HBSS media gradient and then islets were handpicked under the microscope. The islets were cultured in RPMI-1640 medium supplemented

with 10% of FBS prior to use.

2.5.2. Islets encapsulation

The cultured islets were resuspended in 3 wt% of HAMA solution containing 0.2 wt% of LAP, and islets-laden HAMA microgels or islets-laden HAMA@P/C(10) core-shell microgels were prepared according to the aforementioned procedure.

2.5.3. Viability of islets in vitro

To determine islet viability, naked islets and islets-laden HAMA microgels or HAMA@P/C(10) core-shell microgels were added into a 48 well TCPS plate, and incubated for 1, 7 and 14 d. Then calcein AM/ethidium homodimer mixture solution was added to the plates and incubated at 37 °C for 30 min. The samples were imaged under an inverted fluorescence microscope after washing off excess dye. Calcein AM fluoresced green and presented live cells, whereas the ethidium homodimer fluoresced red and indicated dead cells. The viability of islets was defined as the percentage of live cells in total islet cells.

2.5.4. Glucose-stimulated insulin secretion (GSIS)

Naked islets and islets-laden microgels were first cultured in RPMI-1640 media with low glucose concentration (2.8 mM) for 30 min, then transferred into RPMI-1640 media with high glucose concentration (16.7 mM) for 30 min. The supernatants were collected at the end of each incubation and the process was repeated for 4 times incessantly. Quantification of insulin were determined via rat insulin enzyme-linked immunosorbent assay (Rat Insulin ELISA, ALPCO, NH, USA) according to the manufacturer's instructions. In addition, the stimulation index (insulin release at high/low glucose concentration) was calculated for both naked islets and islets-laden microgels.

2.5.5. Inflammatory response

ROS and TNF-α were used as markers to characterize inflammatory response. RAW276.4 macrophages were seeded on the tissue culture plates at a cell density of 100,000 cells/cm^2 and cultured overnight, which were then stimulated with 500 ng mL^{-1} of LPS for 1 h, followed by incubating with naked islets (50 IEQ) or 10% (v/v) of islets-laden microgels for 24 h. Intracellular ROS level was monitored by commercially available assay kit (Beijing Solarbio Science & Technology Co., Ltd), and macrophages treated with 0.05 mg mL^{-1} of Rosup were used as positive control. As for TNF-α, stimulated macrophages were incubated with naked islets or islets-laden microgels for 12 h. The supernatant was collected and the concentration of TNF-α was determined by ELISA kit (Jiangsu Jingmei Biological Technology Co., Ltd, China) following the manufacturer's instructions.

2.6. In vivo characterization of bioartificial pancreas for T1DM treatment

2.6.1. Establishment of the T1DM models

8-week-old C57BL/6J male mice were used to establish T1DM model. To be specific, the mice were intraperitoneally injected with STZ at a dose of 150 mg kg^{-1} after starving overnight. Then non-fasting blood glucose of the mice was measured by collecting blood from the tail vein. Once the blood glucose level was higher than 300 mg dL^{-1} for 3 consecutive days after STZ injection, the mice were then used as T1DM models.

2.6.2. Subcutaneous islets transplantation

A small incision was made at one end of implanted prevascularized scaffold after the diabetic mice were anesthetized, and the silicone tube was stripped from the scaffold. Afterward, islets-laden HAMA@P/C(10) core-shell microgels (500 IEQ) were perfused into the lumen of prevascularized scaffold through a syringe. The incision was closed by suturing and the diabetic mice (n = 4) were allowed to recover. Naked islets or islets-laden HAMA microgels injected into prevascularized scaffold, or naked islets and islets-laden HAMA@P/C(10) microgels injected into subcutaneous space without prevascularized scaffold (n = 3) were used as control groups. Non-fasting glucose of the mice were measured at different time after transplantation.

2.6.3. Intraperitoneal glucose tolerance test (IPGTT) in vivo

To further assess metabolic capacity, IPGTT were conducted at 60 d after transplantation. Mice were fasted overnight before receiving an intraperitoneal glucose bolus (2 g kg^{-1}). The blood glucose levels were monitored at 0, 15, 30, 60, 90 and 120 min after injection (n = 3).

2.6.4. Immunofluorescence staining of insulin

To perform immunofluorescence staining of retrieved bioartificial pancreas, the histological sections were incubated with primary antibodies (mouse anti-insulin, Boster, China) and fluorescent secondary antibodies (Alexa Fluor 488 donkey anti-mouse IgG, Abcam, England) successively. The sections were further stained with DAPI staining (Beyotime, China) before observation under an inverted fluorescence microscope.

2.7. Statistical analysis

Data were presented as means ± standard deviations (SD). One-way analysis of variance (ANOVA) was applied to calculate the differences between values. Values of $p < 0.05$ were considered as statistically different. Levels of significant difference were presented as * ($p < 0.05$), ** ($p < 0.01$) and *** ($p < 0.001$).

3. Results and discussion

3.1. Fabrication and characterization of macroscale hydrogel scaffold

Subcutaneous islets transplantation is very attractive clinically, considering its convenience for implantation and retrieval, ease for graft monitoring, and low-risk for surgical complications. However, inadequate vascularization of the subcutaneous space results in poor oxygen and nutrient supplement to the transplanted islets, limiting its application as a suitable transplantation site. As such, establishment of subcutaneous vasculature is necessary for islet transplantation. Given the role of vascular endothelial growth factor (VEGF) in angiogenesis [44], a new hydrogel scaffold containing methacrylated gelatin (GelMA), methacrylated heparin (HepMA) and VEGF was developed. HepMA in hydrogel scaffold provides abundant binding sites for VEGF [45], enabling the sustained release of VEGF to recruit endothelial cells. GelMA is a modified natural polymer with good biocompatibility and biodegradability [46–48], which can offer a certain mechanical support for the new-born blood vessels in the early period of islets transplantation and degrade later to reduce the distance between new-born blood vessels and islets-laden microgels.

Fig. 1a depicts schematically the preparation process of this scaffold. In brief, a biomedical silicone tube was soaked in GelMA/HepMA hydrogel precursor solution, and ice water was injected into the tube through a syringe. Conformal hydrogel layer was condensed on the tube surface due to gelation of GelMA at low temperature [49,50], which was then irradiated with blue light for photopolymerization of GelMA and HepMA. The scaffold was finally acquired by immersing in VEGF solutions, where VEGF was loaded into the hydrogel tube and bound to HepMA owing to their strong biological affinity. Fig. 1b gives the photos corresponding to the process shown in Fig. 1a. Notably, the silicone tube could be withdrawn from the as-formed hydrogel tube, leaving a chamber for islets transplantation (Fig. S1). Fig. 1c compares the heparin and HepMA stability in hydrogel scaffold. The numbers in GelMA/HepMA2.5, GelMA/Heparin2.5, and GelMA/Heparin5.0 represent the mass percentage of heparin and HepMA in hydrogels. After staining with toluidine blue, GelMA/HepMA2.5 and GelMA/Heparin2.5 hydrogels exhibit characteristic blue-purple color, indicating the presence of heparin and HepMA [51]. Meanwhile, the blue color of stained GelMA

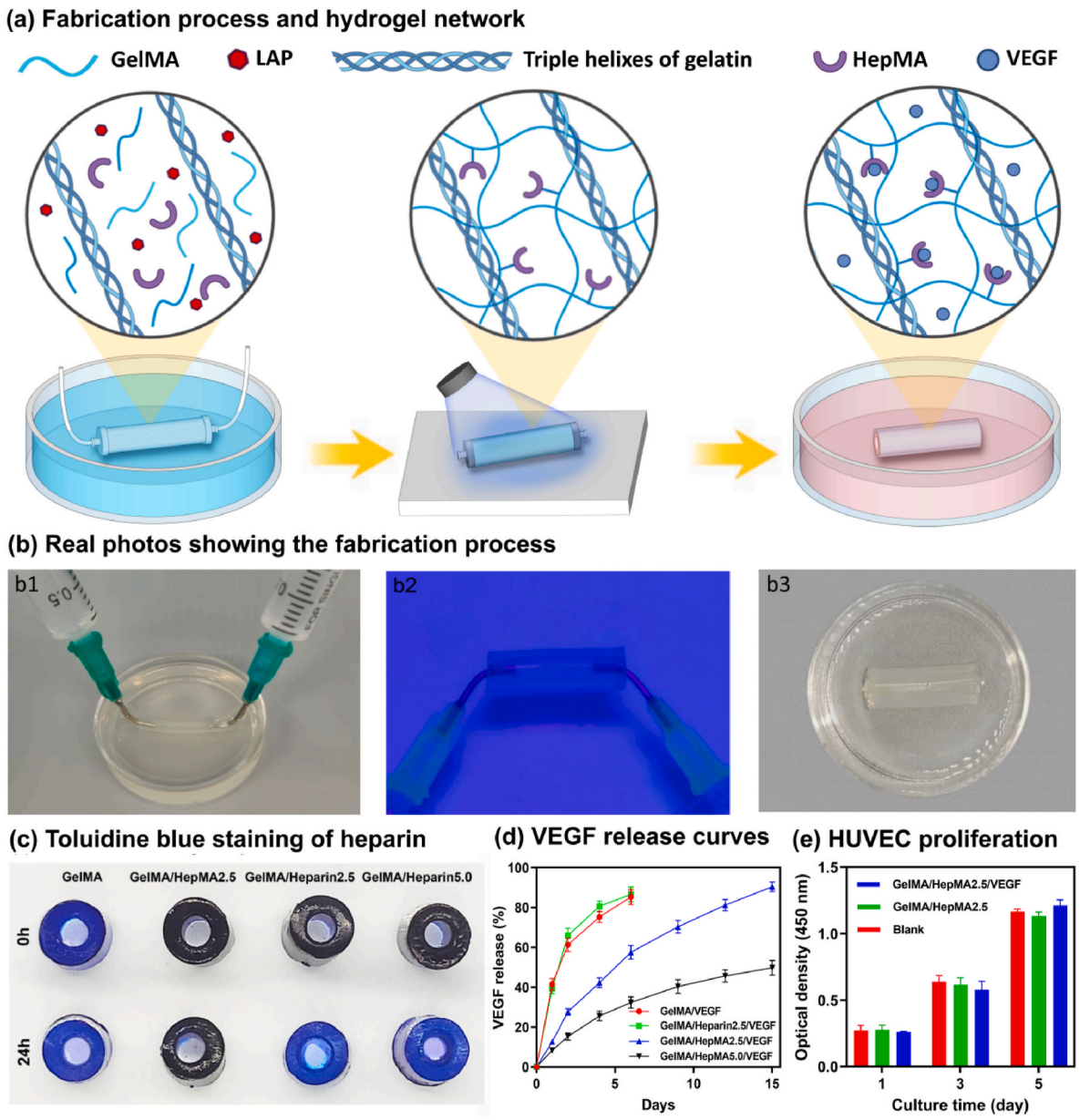

Fig. 1. Preparation and characterization of GelMA/HepMA/VEGF hydrogel scaffold. a) schematics on the fabrication process and hydrogel network of GelMA/HepMA/VEGF hydrogel scaffold; b) photos illustrating the step-by-step fabrication process; c) toluidine blue staining of heparin; d) VEGF release behaviors from hydrogel scaffolds; e) HUVEC proliferation on hydrogel surfaces.

hydrogel is only caused by toluidine blue itself. Furthermore, no noticeable color change can be observed in the GelMA/HepMA2.5 hydrogel after immersing in PBS for 24 h, proving that HepMA is very stable in scaffold owing to the covalent crosslinking between GelMA and HepMA. In contrast, GelMA/Heparin2.5 hydrogel changes from the blue-purple color at 0 h to the blue color at 24 h, suggesting the release of heparin from the hydrogel scaffold. Even doubling of the heparin amount in the scaffold cannot avoid the color fading, or namely, the quick release of heparin. Fig. 1d lists the VEGF-releasing curves of various hydrogel scaffolds including GelMA/VEGF (prepared by immersing GelMA hydrogel in VEGF solution), GelMA/Heparin/VEGF (prepared by immersing GelMA/Heparin hydrogel in VEGF solution) and GelMA/HepMA/VEGF (prepared by immersing GelMA/HepMA hydrogel in VEGF solution). As expected, over 60% of the loaded VEGF is released from GelMA/VEGF and GelMA/Heparin2.5/VEGF hydrogel scaffolds within 2 days, whilst a sustained release of VEGF up to 15 days is observed for GelMA/HepMA2.5/VEGF hydrogel scaffold. When the HepMA content increases in GelMA/HepMA/VEGF hydrogel, the sustained release of VEGF can be observed more obviously. It can be conceived that there are three types of VEGF in the above three hydrogels, including free VEGF, VEGF/Heparin complex and VEGF/-HepMA complex. Since the free VEGF and VEGF/Heparin complex dissolved in water can be quickly released from hydrogel, the sustained release of VEGF is only achieved by VEGF/HepMA complex, owing to the stability of HepMA in GelMA/HepMA/VEGF scaffold. Therefore, although the VEGF loading capacities are similar for GelMA/HepMA/-VEGF, GelMA/Heparin/VEGF and GelMA/VEGF hydrogels, their sustained release of VEGF are quite different. Considering the subcutaneous angiogenesis can be achieved in 15 days [52,53] and GelMA/-HepMA2.5/VEGF can realize VEGF sustained release in this period, GelMA/HepMA2.5/VEGF hydrogel scaffold is used for the following experiments.

The cytocompatibility of GelMA/HepMA and GelMA/HepMA/VEGF scaffolds were further evaluated by seeding human umbilical vein

endothelial cells (HUVECs) on the two hydrogel surfaces. Live/dead staining in Fig. S2 and CCK-8 assay in Fig. 1e suggest that no significant difference of HUVEC viability and proliferation occurs between control group and hydrogel scaffolds after 1, 3 and 5 days of culture, demonstrating good cytocompatibility of these two hydrogel scaffolds.

3.2. In vitro and in vivo angiogenesis of GelMA/HepMA/VEGF hydrogel scaffold

The recruitment ability of GelMA/HepMA/VEGF scaffold to endothelial cells was firstly assessed by in vitro transwell migration assay, where HUVECs were seeded in the transwell chamber and GelMA/HepMA/VEGF scaffold was placed in 24-well plate chamber. It can be found from Fig. 2a that the HUVECs migrated onto the GelMA/HepMA/VEGF scaffold after 12 h is remarkably more than those on blank and GelMA/HepMA scaffold, indicative of the critical role of released VEGF in the HUVEC migration (see quantitative data in Fig. S3). Subsequently, the GelMA/HepMA/VEGF scaffold (outer diameter: 5.0 mm, length: 20.0 mm, wall thickness: 1.0 mm) was implanted subcutaneously to verify the angiogenesis performance in vivo. As shown in Fig. 2b, no obvious blood capillaries can be observed on silicone tube after implantation for 15 days, while lots of blood capillaries are seen clearly on the surface of GelMA/HepMA/VEGF scaffold. This observation was further confirmed by hematoxylin & eosin (H&E) staining and CD31 immunohistochemical analysis. The H&E staining in Fig. 2c reveals that only a few hollow lumens (marked by blue arrows) are found around the retrieved silicone tube. In comparison, much more hollow lumens are visible nearby for the retrieved GelMA/HepMA/VEGF scaffold, suggesting its excellent angiogenesis performance. The presence of erythrocytes in these hollow lumens proves the anastomosis between the new-born capillaries and the host blood vessels [54]. Besides, the number of inflammatory cells close to GelMA/HepMA/VEGF scaffold are not high on day 15 (orange arrows in Fig. 2c) compared with that on day 7 (orange arrows in Fig. S4), which means that the acute inflammatory response subsides and the hydrogel scaffold is of sound histocompatibility. Furthermore, subcutaneous angiogenesis of GelMA/HepMA and GelMA/Heparin/VEGF scaffolds were also investigated in vivo. The new-born blood vessels found around GelMA/HepMA and GelMA/Heparin/VEGF scaffold is much less than that of GelMA/HepMA/VEGF scaffold (Fig. S5). The result suggests that neither the hydrogel scaffold itself nor the burst release of VEGF from the scaffold can induce the formation of substantial blood vessels, further proving the important role of sustained-release VEGF on angiogenesis. CD31, a characteristic protein expressed on the surface of vascular endothelial cells, is often used to indicate the new-born blood vessels [55,56]. The CD31 staining results in Fig. 2d show the similar outcome like H&E staining, i.e., sparse blood capillaries for silicone tube and dense blood capillaries for GelMA/HepMA/VEGF scaffold (marked by red arrows). The vascular density, defined as the percentage of vascular area in total field, exhibits in a quantitatively way the outstanding angiogenesis induced by GelMA/-HepMA/VEGF scaffold (Fig. 2e). More importantly, all retrieved scaffolds can maintain their initial shape without deformation in vivo due to the presence of silicone tube, and hence reserve the inner lumen as transplantation site for islets-laden microgels.

3.3. Preparation and characterization of core-shell microgels

In our study, core-shell microgels for islets microencapsulation were prepared via two steps. First, mono-core microgels were generated through a droplet-based microfluidic device (Fig. S6), in which aqueous droplets were produced continuously under the shear stress of the oil phase and converted into mono-core microgels after photopolymerization [57–61]. Next, the as-prepared mono-core microgels were loaded with photoinitiator by immersing them into LAP solution for a short time. After transferring these mono-core microgels into another hydrogel precursor solution, the absorbed LAP diffused outward from the mono-core microgels, triggering the photopolymerization reaction on the mono-core microgel surface by blue light irradiation and thus leading to the formation of core-shell microgels (Fig. 3a). Obviously, the hydrogel precursor far away from the microgels cannot be polymerized due to the lack of LAP. Compared with the fabrication methods reported in the literature for core-shell microgels, our method is easy to control especially for microfluidic operation and the thickness of core and shell layers can be adjusted separately [62,63].

To prove the universality of our method and successful preparation of core-shell microgel, several popular hydrogel materials, including methacrylated hyaluronic acid (HAMA), GelMA, poly(ethylene glycol) diacrylate (PEGDA), were used as either core or shell materials. It is found that the thickness of shell layer in the core-shell microgel is variable, mainly depending on the diffusion time of initiator and the precursor concentration of shell materials. Fig. 3b shows the optical image of GelMA@PEGDA microgels with thick shell layer (diffusion time of initiator: 2 min, thickness of shell layer: ~50 μm). Notably, to reduce the delay of thick shell layer on nutrient/insulin exchange, thin shell was actually used for islet microencapsulation (diffusion time of initiator: 30 s, thickness of shell layer: ~5 μm). For the sake of observing thin shell layer in core-shell microgels, fluorescent aminofluorescein grafted HAMA (HAMA-AF, green light) or fluorescent PS microspheres-loaded PEGDA (blue light) were alternatively adopted. Specifically, the core and shell of HAMA@PEGDA, shell of both GelMA@HAMA and GelMA@PEGDA are of fluorescence. As can be seen in Fig. 3b, the uniformity of the shell layer is proven by the fluorescent illumination of the shell layer in HAMA@PEGDA, GelMA@HAMA and GelMA@PEGDA microgels, suggesting that the thin shell layer is fully wrapped on the core-shell microgels. Interestingly, our strategy can be further extended to fabricate multilayer core-shell microgels (labelled as core-shell*n, n is the layer number of shells). As observed in Fig. 3c, the HAMA mono-core microgels prepared via droplet-microfluidics are monodisperse with round shape and their average size is 310.48 ± 6.85 μm. After immersing HAMA mono-core microgels in LAP solution and then exposing them to blue light in PEGDA precursor solution, the average size of HAMA@PEGDA core-shell microgels increases to 321.67 ± 7.51 μm. Repetition of the same procedure for shell formation makes the HAMA@PEGDA core-shell*2 microgels bigger (333.64 ± 6.96 μm). Although core-shell*2 microgels with different shell components are not available now, it is obvious that our method is suitable for fabricating them so that more complicated functions can be achieved.

3.4. Anti-adhesion performance of core-shell microgels

When exogenous cells/materials are implanted into the human body, the complement system (including various types of proteins) is activated through the surface adsorption of complement proteins. When the implants are too large to be swallowed, macrophages can fuse to form foreign body giant cells, secrete cytokines to collect and integrate fibroblasts to deposit matrix, and finally wrap the implants with avascular collagen capsules. This dense fibrotic capsule isolates the implants from the internal circulation system of the body, cuts off the exchange of substances, and causes necrosis of the implant [64,65]. Therefore, the inhibition of protein and macrophages adhesion on implants can effectively reduce the risk of implantation failure. Herein, FITC-BSA was chosen as a model protein to evaluate the protein adhesion on different bulk hydrogel materials (Fig. 4a and S7). Among all the hydrogel materials studied herein, GelMA shows the highest protein adhesion amount, indicative of the most severe immunogenicity after implantation. In comparison, HAMA and PEGDA mitigate to some extent the protein adhesion, possibly due to their higher hydrophilicity. To minimize the protein adhesion, zwitterionic carboxybetaine methacrylate (CBMA), as a strong antifouling material [66,67], was synthesized and verified by the ^{1}H NMR spectrum in Fig. S8. Since it is time-consuming for the gelation of pure CBMA, copolymerization of PEGDA and CBMA was used instead. The formation of PEGDA/CBMA hydrogel

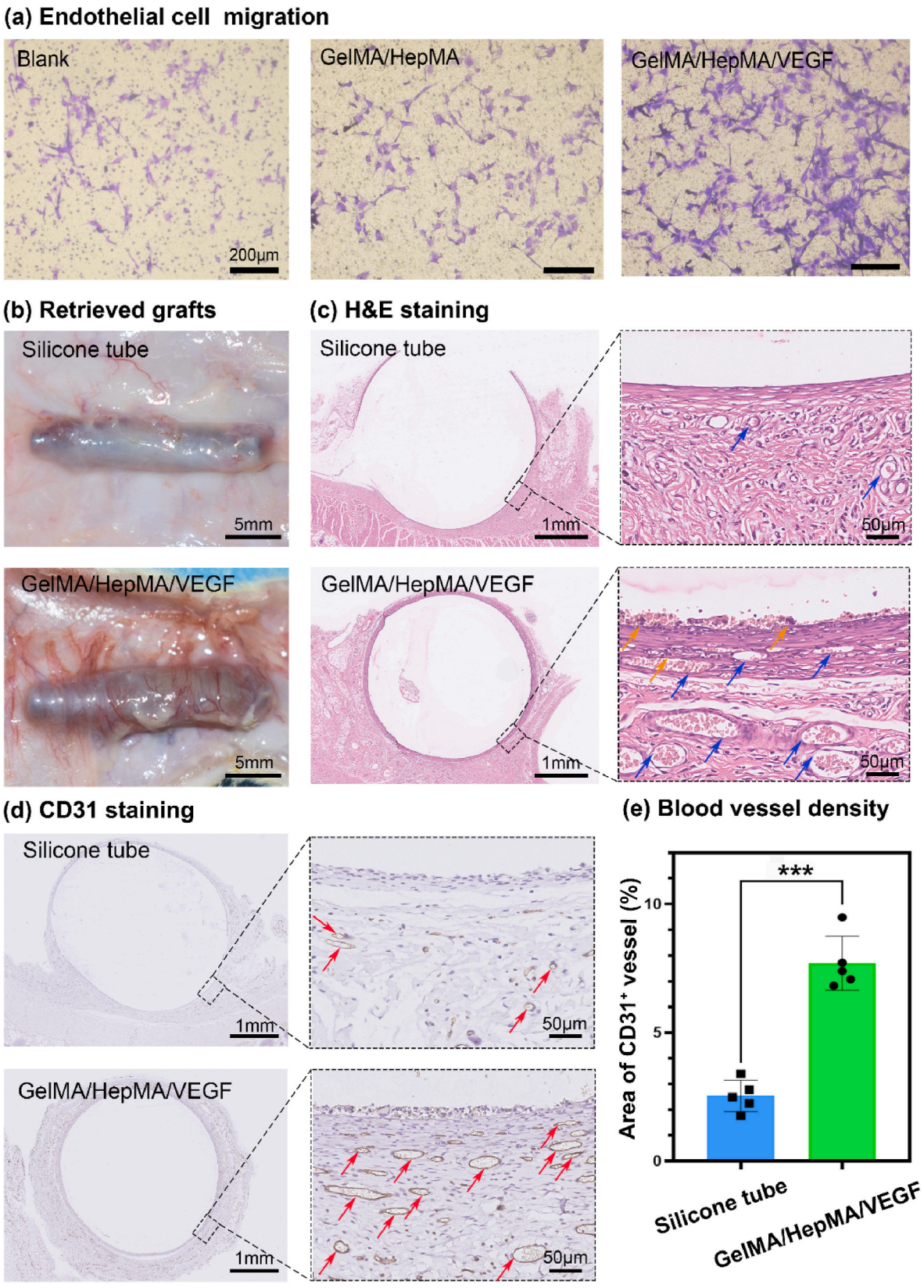

Fig. 2. In vitro and in vivo angiogenesis of GelMA/HepMA/VEGF scaffold. a) recruitment ability of GelMA/HepMA/VEGF scaffold to endothelial cells assessed by in vitro transwell migration assay; b) photos of retrieved silicone tube and GelMA/HepMA/VEGF scaffold after subcutaneous implantation for 15 days; c) H&E staining of retrieved hydrogel scaffolds. Blue arrows indicate the location of new-born blood capillaries and orange arrows indicate the location of inflammatory cells; d) CD31 immunohistochemical staining of retrieved hydrogel scaffolds. Red arrows indicate the location of new-born blood capillaries; e) vascular density of the silicone tube and GelMA/HepMA/VEGF scaffold. Five different locations were selected for calculation (n = 5).

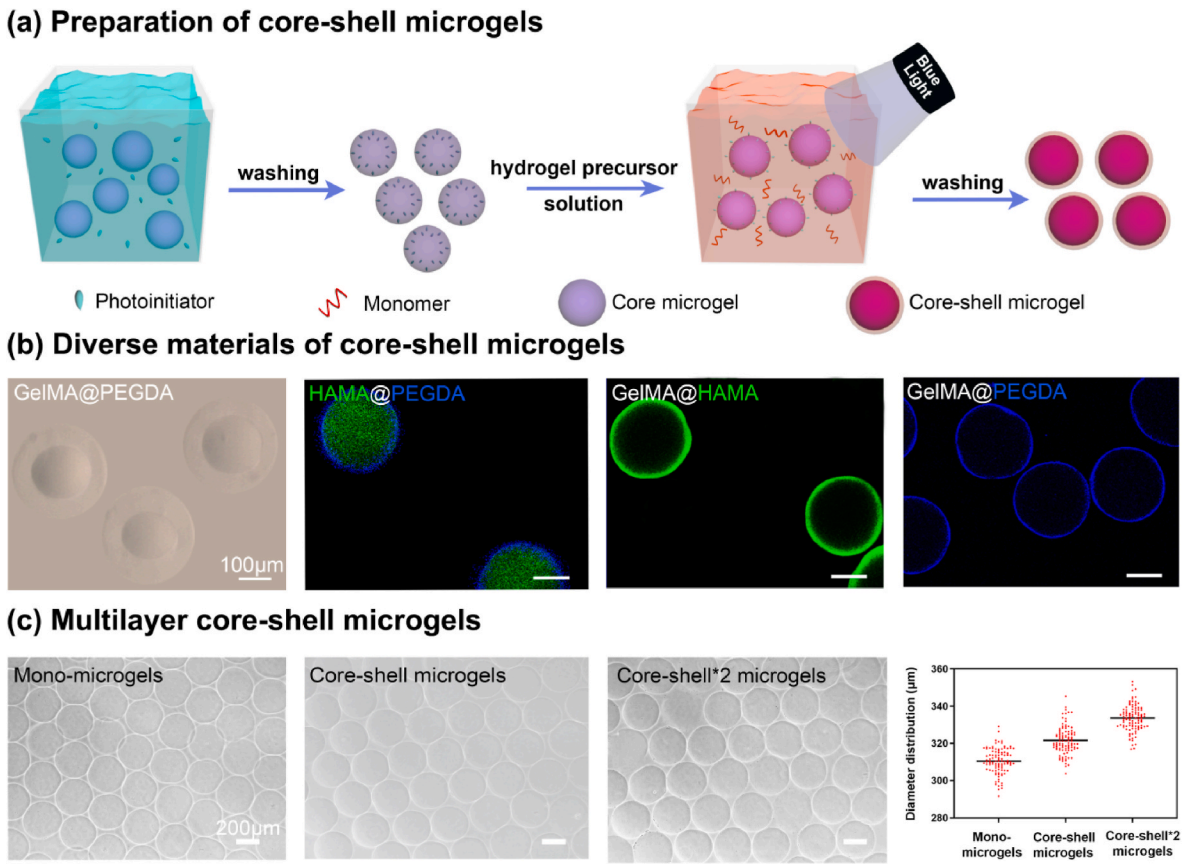

Fig. 3. Preparation and characterization of core-shell microgels. a) schematic illustration on the preparation of core-shell microgels from mono-core microgels; b) bright-field and fluorescence images of core-shell microgels with various core and shell materials; c) multilayer core-shell microgels (from left to right: mono-core microgels, core-shell microgels, core-shell*2 microgels).

(abbreviated as P/C hydrogel) is confirmed via FTIR (Fig. S9), where the characteristic peaks at 2880 cm^{-1} and 1100 cm^{-1} can be assigned to the stretching vibration of –CH and C–O–C in PEGDA, and the adsorption bands at 1590 cm^{-1} and 1171 cm^{-1} can be attributed to the stretching vibration of carbonyl and methacryloyl groups in CBMA, respectively. It is evident that the protein adsorption capacities of P/C hydrogels are much lower than those of GelMA, PEGDA and HAMA hydrogels. When the CBMA content is greater than 10 wt%, the prepared P/C hydrogel has the maximum anti-adhesion effect. What's more, CBMA content also affects the swelling properties and porosity of P/C hydrogels, i.e., the more the CBMA content is, the higher the swelling ratio and porosity of P/C hydrogel possesses (Fig. 4b and c). Except for bulk hydrogels, the anti-adhesion performance was also tested using microgels. It is apparent that HAMA@P/C(10) microgels display lower protein adsorption compared with HAMA and HAMA@PEGDA microgels (Fig. 4d), in good agreement with the results of bulk hydrogels. Noteworthily, the anti-adhesion ability of the HAMA@P/C (10) microgels is not only reflected on proteins, but also on macrophages. As shown in Fig. 4e, the adsorption amounts of macrophages decrease in turn from HAMA, HAMA@PEGDA and HAMA@P/C(10) microgels, and almost no macrophages are observed on HAMA@P/C(10) microgel surface. Such results were further validated via in vivo subcutaneous transplantation of HAMA@P/C(10) microgels, where few immunocytes are found around HAMA@P/C (10) microgels after transplantation for 3 days (Fig. S10). Taking into account the anti-adhesion performance of shell hydrogel and the cytocompatibility of core hydrogel required in our case, P/C(10) and HAMA hydrogels are selected as the shell and core materials for the following experiments and their porous structure are confirmed by scanning electron microscopy (SEM, Fig. S11).

3.5. *In vitro biological characterization of islets-laden HAMA@P/C(10) microgels*

To fabricate islets-laden HAMA@P/C(10) microgels, naked islets were firstly isolated from male SD rats according to the protocol used in our previous work [68]. Fig. S12a gives the photo of isolated islets, whose average size is 111.24 ± 20.09 μm. The islets-laden HAMA@P/C (10) microgels were then prepared using the same method described in Section 3.3. Precise control of the islets concentration in water phase as well as the flow rates of water and oil phases can make islets distribute uniformly in microgels, as shown in Fig. S12c. The full coverage of P/C shell on HAMA microgel surface is confirmed using zeta potential measurement, i.e., islets-laden HAMA microgels show a zeta potential of −49.50 ± 4.71 mV, whereas islets-laden HAMA@P/C(10) microgels exhibit a zeta potential of −1.41 ± 0.53 mV (Fig. S13). In addition to the enhanced anti-adhesion and hence suppressed host immune rejection, the P/C(10) hydrogel shell also endows the encapsulated islets with better mechanical protection since the mechanical strength of P/C(10) hydrogel is significantly higher than that of HAMA (Fig. S14). This feature of HAMA@P/C(10) microgel is very favorable for islets transplantation, as the HAMA core can provide a biomimetic soft microenvironment for islets and simultaneously the P/C shell can bear the shear force generated during microgel injection and human motion post implantation.

Islets viability and insulin-secretion function in HAMA@P/C(10) microgels were explored via live/dead staining and glucose-stimulated insulin secretion (GSIS) test. As can be seen in Fig. 5a, naked islets show high cell viability on the 1st and 7th days after isolation from SD rats, but a small part of islets are necrotic in the center of islet cluster on the 14th day (see separate fluorescence images of live islets and dead

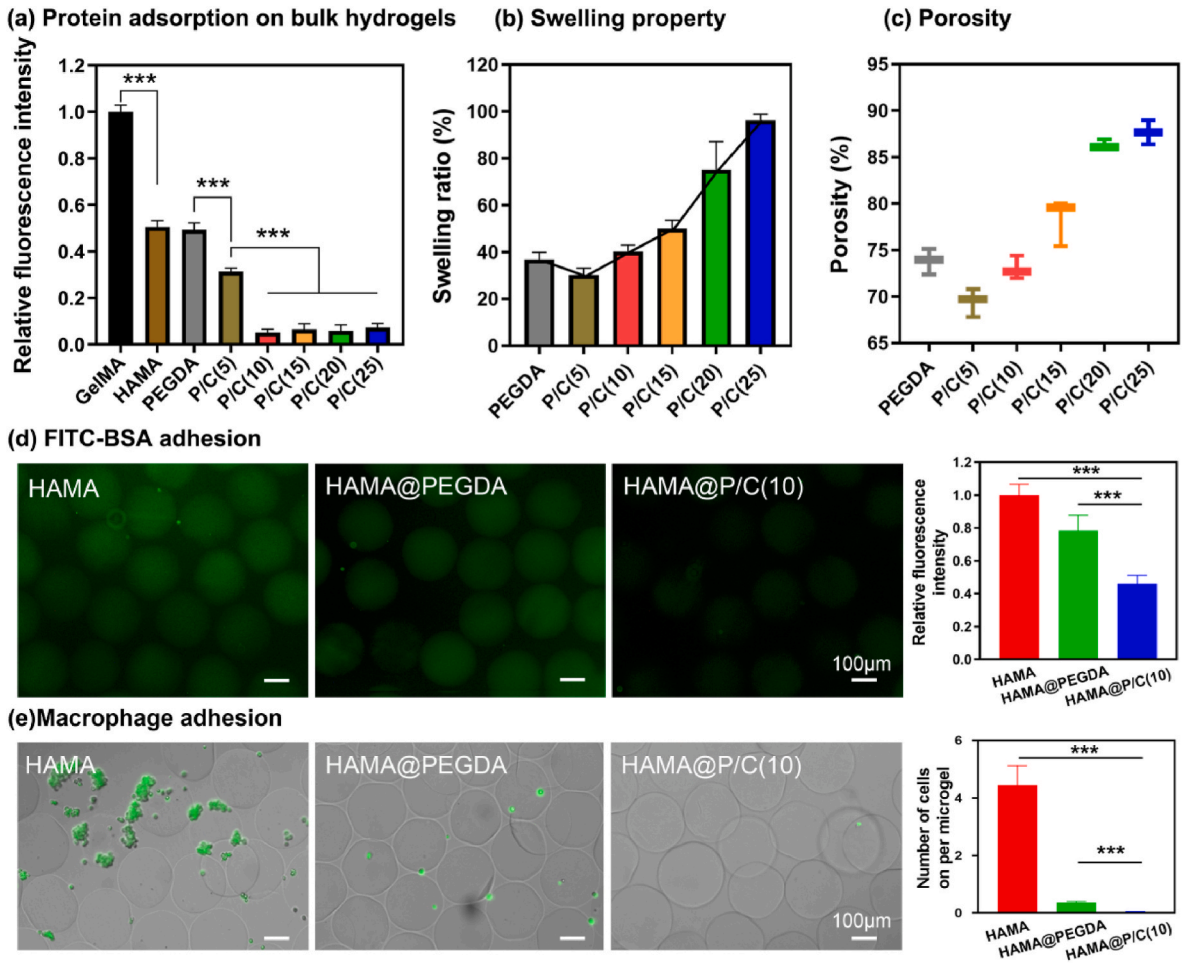

Fig. 4. Anti-adhesion performance of core-shell microgels: a) protein adsorption on the surface of bulk hydrogels. The relative fluorescence intensity of bulk hydrogels was normalized by the fluorescence intensity of GelMA hydrogel; b) swelling properties of bulk hydrogels; c) porosity of bulk hydrogels; d) protein adsorption on microgels. The relative fluorescence intensity of microgels was normalized by the fluorescence intensity of HAMA microgels; e) macrophage adhesion on microgels.

islets in Fig. S15). This is possibly due to the physiological difference between in vivo and in vitro, such as the absence of dynamic culture in vitro [69,70]. The poor proliferation rate of islets lead to an increased proportion of necrotic cells with culture time [71,72]. Fortunately, there is no significant difference in cell viability between naked islets and the islets encapsulated in HAMA and HAMA@P/C(10) microgels, implying that islets microencapsulation in HAMA microgels via microfluidic technology and construction of P/C(10) hydrogel shell outside the HAMA microgels have negligible effects on islets viability (see quantitative data in Fig. S16). In addition, when naked islets are switched between high glucose (16.7 mM) and low glucose (2.8 mM) solutions, their insulin secretion increases and decreases correspondingly (Fig. 5b). The stimulation index (SI), a ratio of insulin secreted at high glucose concentration to that of low glucose concentration, is 2.31 ± 0.21. Encapsulation of islets in HAMA and HAMA@P/C(10) microgels doesn't change their sensitivity to glucose. After continuous 4 cycles, their stimulation indexes still maintain at 2.23 ± 0.07 and 2.17 ± 0.11 respectively, indicating that our islets microencapsulation strategy has no significant negative effect on islets activity and insulin-secretion function.

Inflammatory response of islets-laden HAMA@P/C(10) microgels was assessed via co-culturing them with macrophages (RAW264.7 cells) and monitoring reactive oxygen species (ROS) and tumor necrosis factor-α (TNF-α) levels [73]. Fig. 5c shows the fluorescence images of ROS detection and related statistical data. The naked islets group produces a high level of ROS, as Rosup group (positive control) does, implying the extraordinarily active inflammatory response of macrophages to xenogeneic islets. Compared to naked islets, two microgel groups especially HAMA@P/C(10) microgel group induce much lower inflammatory response, as a result of the good anti-adhesion of P/C(10) shell. Even after encapsulation of islets in HAMA@P/C(10) microgels, the inflammatory response of macrophages doesn't change significantly, mainly owing to the shielding of core-shell microgels to islets. Apart from ROS, TNF-α was also tested and the results are in good accordance with those of ROS measurement, i.e., islets-laden HAMA@P/C(10) microgels don't trigger severe inflammatory response (Fig. 5d).

3.6. *Xenotransplantation of bioartificial pancreas in vivo*

The new bioartificial pancreas developed in this work consists of a prevascularized hydrogel scaffold and islets-laden core-shell microgels. Considering that in vivo prevascularization of the hydrogel scaffold needs a period of time, xenotransplantation of this bioartificial pancreas was performed by two steps: the GelMA/HepMA/VEGF hydrogel scaffold containing silicone tube was first subcutaneously implanted in diabetic mice, sutured and prevascularized for 15 days. Thereafter, the silicone tube was removed out from the prevascularized hydrogel scaffold and islets-laden HAMA@P/C(10) microgels were injected into the lumen of hydrogel scaffold (Fig. 6a). As a result, the new-born blood vessels can supply oxygen and nutrients for islets promptly. Six groups

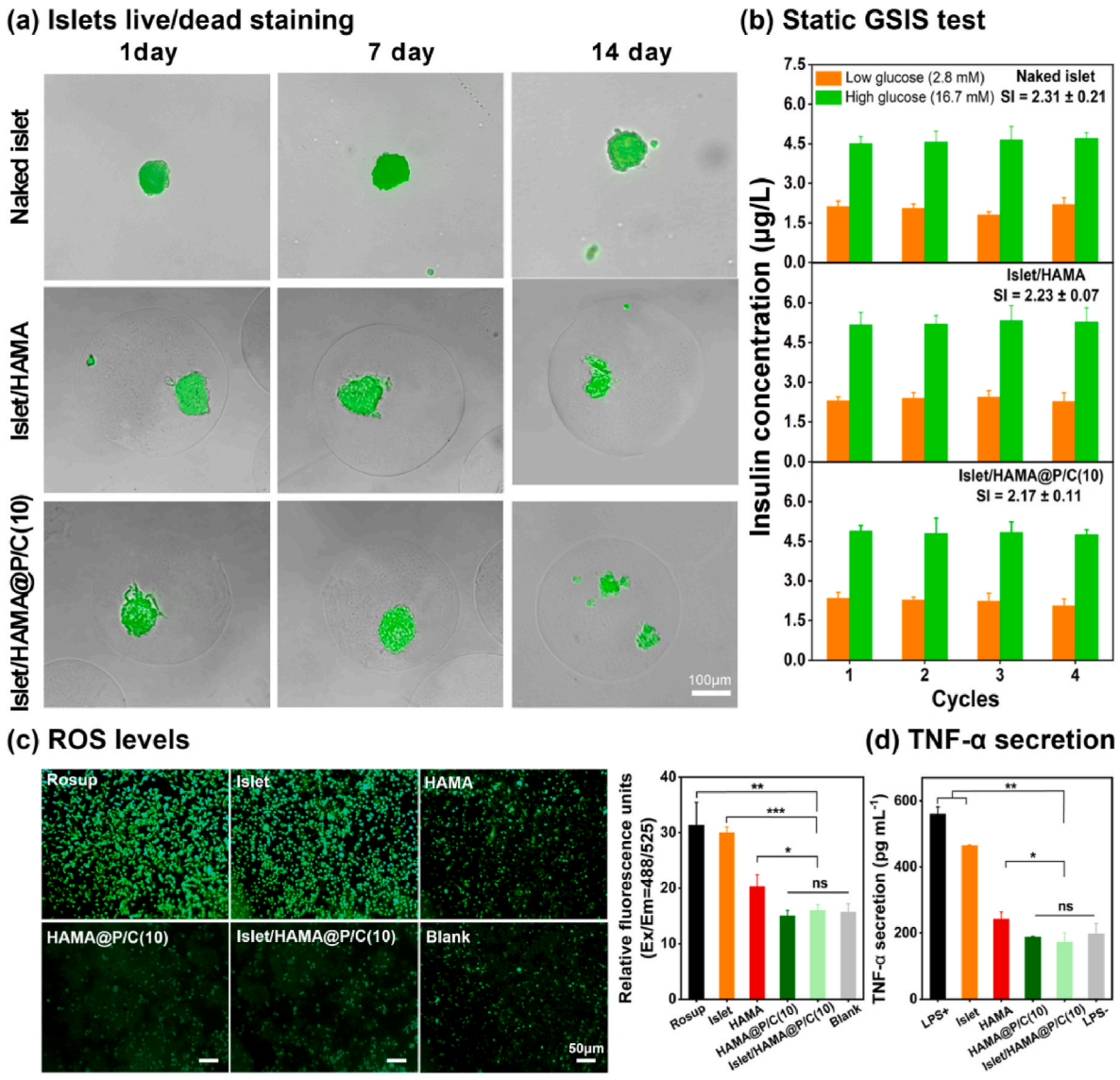

Fig. 5. In vitro biological characterization of islets-laden HAMA@P/C(10) microgels: a) islets viability via live/dead staining; b) insulin-secretion via glucose-stimulated insulin secretion (GSIS) test; c) ROS level and d) TNF-α level generated by macrophages after co-culturing with islets-laden HAMA@P/C(10) microgels. 50 islet equivalents (IEQ) of SD rats were used for naked islets and islets-laden HAMA@P/C(10) groups.

(four duplicates for experimental group and three duplicates for other groups), including prevascularized scaffold and islets-laden HAMA@P/C(10) microgels, prevascularized scaffold and islets-laden HAMA microgels, prevascularized scaffold and naked islets, islets-laden HAMA@P/C(10) microgels, naked islets, diabetic mice, were tested simultaneously. 500 islet equivalents (IEQ) of SD rats were used for each group if applicable, following the protocol in the literarure (Table S1). Fig. 6b shows the random non-fasting blood glucose levels (BGLs) monitored every 2 days. After injecting streptozotocin in normal mice for 3 days, their BGLs rise and maintain continuously above 300 mg dL^{-1}, indicating the successful construction of diabetic mice models. At day 4 following transplantation into diabetic mice, the prevascularized scaffold and islets-laden HAMA@P/C(10) microgels group (or namely, bioartificial pancreas) demonstrates a rapid reversal of BGLs from hyperglycemia (>300 mg dL^{-1}) to normoglycemia (<200 mg dL^{-1}), and holds the normal BGL for up to 90 days. However, direct hypodermic injection of islets-laden HAMA@P/C(10) microgels can only lead to a small drop of BGLs, which rebound quickly back to its original level. This validates the important role of the prevascularized scaffold in bioartificial pancreas. According to the results in Section 3.2, a rich vascular network is formed around the GelMA/HepMA/VEGF scaffold after transplanting it for 15 days. It is believed that the new-born vascular network increases dramatically the subcutaneous oxygen content, leading to the high islets viability especially in the early period of islets transplantation. Islets in islets-laden HAMA@P/C(10) microgels group become apoptotic rapidly due to the lack of oxygen and nutrient supply from surrounding environment, resulting in the failure of transplantation. Besides, compared with bioartificial pancreas group, transplantation of naked islets into the prevascularized scaffolds can achieve a short period of normoglycemia for 1–3 days and then return to hyperglycemia. The possible reason lies in the immune system attack caused by xenogeneic islets transplantation. To prove this assumption, islets-laden HAMA microgels were also transplanted into the prevascularized scaffold, which physically shields islets from host immune system. It can be noticed that much longer period of normoglycemia (ca. 36–42 days) can be achieved. Obviously, the physical protection is further enhanced by introducing anti-adhesion core-shell microgels. Since neither physical protection nor new-born blood capillaries are available, naked islets group exhibits the worst transplantation effect.

Prior to graft retrieval, in vivo intraperitoneal glucose tolerance tests

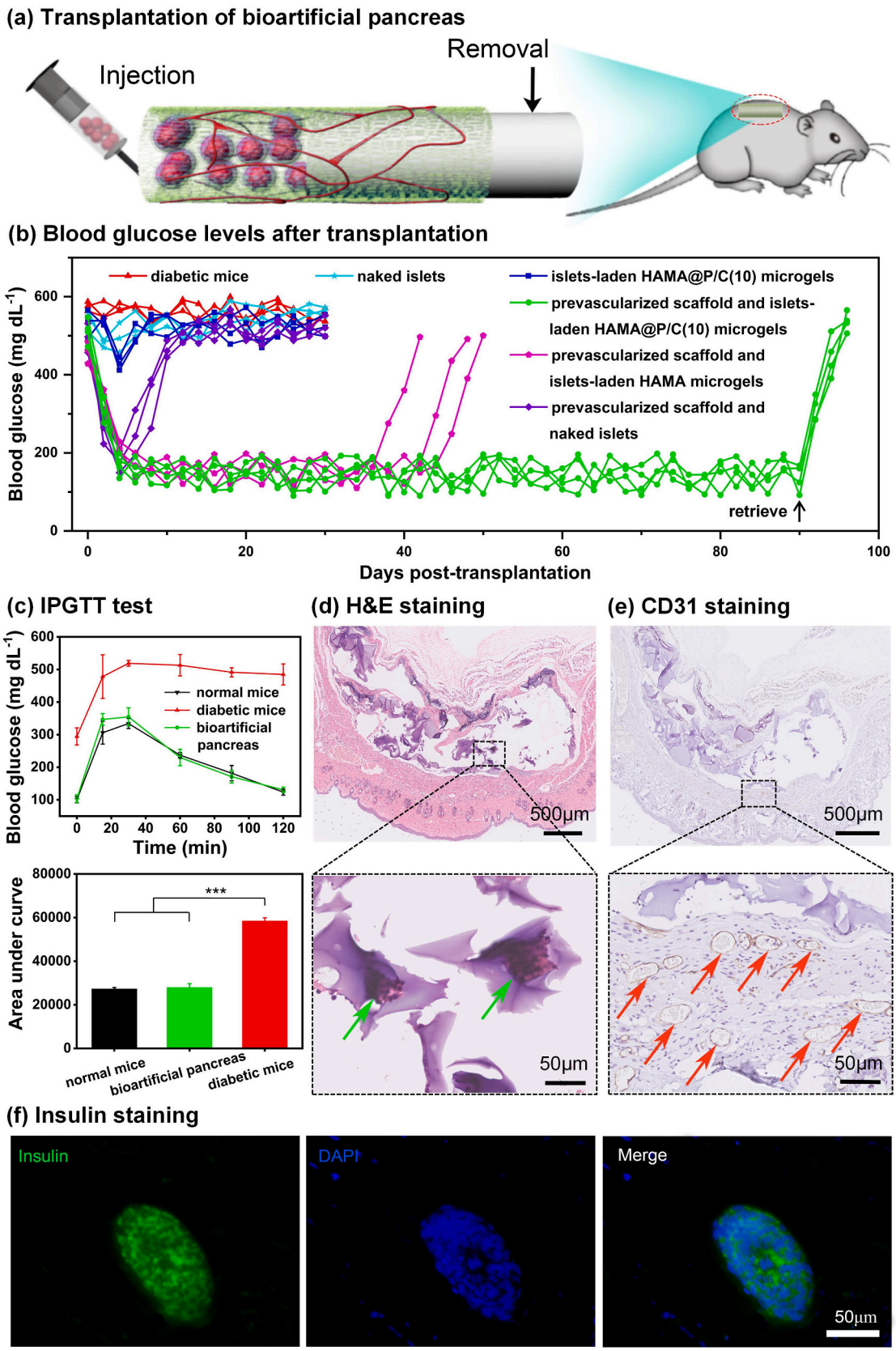

Fig. 6. Subcutaneous transplantation of bioartificial pancreas into STZ-induced diabetic mice: a) schematic illustration of islets transplantation process; b) in vivo BGLs post transplantation; c) intraperitoneal glucose tolerance test (IPGTT); d) H&E staining of retrieved bioartificial pancreas 90 days post transplantation; e) CD31 immunohistochemical staining and f) insulin immunofluorescence staining of retrieved bioartificial pancreas 90 days after transplantation.

(IPGTTs) were conducted to check the real-time response of bioartificial pancreas to glucose. Fig. 6c shows that diabetic mice after transplantation of bioartificial pancreas have the same dynamic response as normal mice, whilst diabetic mice without bioartificial pancreas are difficult to decrease BGL, which is also quantified by their metabolic capacity (area under curve, Fig. 6c). Thereafter, the bioartificial pancreas was retrieved at day 90 post-transplantation by surgery, accompanying with an immediate increase in BGLs of diabetic mice. This phenomenon proves the long-term viability and blood glucose regulation function of islets in bioartificial pancreas. H&E staining of the retrieved bioartificial pancreas in Fig. 6d reveals that the microencapsulated islets (marked by green arrows) are intact in shape and no leakage of islets-laden microgels from the prevascularized scaffold is observed. More importantly, the microgel surface is still clean at 90 days after transplantation, and no obvious macrophage deposition and fibrous capsule formation are observed, illustrating their antifibrotic ability. CD31 immunohistochemical staining in Fig. 6e corroborates again the high blood vessel density in the prevascularized scaffold. The negligible distance between the new-born blood vessels (marked by red arrows) and lumen of hydrogel scaffold implies the biodegradation of hydrogel scaffold, which facilitates the supply of oxygen and nutrients to islets-laden HAMA@P/C(10) microgels. Meanwhile, immunofluorescence staining of insulin (Fig. 6f) confirms that the retrieved islets still remain insulin-secretion function at day 90 after transplantation [74,75].

In addition, to verify the role of prevascularization in vivo on islet transplantation, simultaneous transplantation of hydrogel scaffold (with or without VEGF) and islets-laden microgels was also performed. In other words, another two control groups (unprevascularized GelMA/HepMA/VEGF scaffold and islets-laden HAMA@P/C(10) microgels, unprevascularized GelMA/HepMA scaffold and islets-laden HAMA@P/C(10) microgels) were tested. As shown in Fig. S17a, BGLs in these two groups show a very short decrease at the early stage after islet transplantation, and rebound to original hyperglycemia state on day 8. Although GelMA/HepMA/VEGF scaffold can induce abundant new-born blood vessels on day 16 after subcutaneous transplantation compared with GelMA/HepMA scaffold (Fig. S17b), the transplanted islets show very weak insulin-secretion function (Fig. S17c). This is possibly because the unprevascularized GelMA/HepMA/VEGF scaffold fails to provide enough nutrient/oxygen to transplanted islets especially in the early stage of transplantation and the resulting hypoxia causes the death of many islets, which confirms the important role of prevascularization in vivo.

In brief, the data described above, including the monitoring of BGLs, H&E staining, CD31 immunohistochemical staining and insulin immunofluorescence staining of retrieved graft, suggest sufficiently that our bioartificial pancreas, i.e., islets microencapsulation in anti-adhesive core-shell microgels and macroencapsulation in a prevascularized scaffold, can maintain islets viability in vivo and ensure the insulin secretion of islets to regulate the BGLs. Notably, herein 500 islet equivalents were transplanted into the prevascularized hydrogel scaffold with the total volume of 0.4 mL (outer diameter: 5.0 mm; length: 20.0 mm). This means that a device with the total volume of 200 mL should be implanted in order to accommodate sufficient islets (~5000 IEQ/kg, 50 kg). Although the calculated hydrogel device is larger than natural pancreatic tissue (~100 mL) [76], it can be further improved by decreasing the blank microgels and thus reducing the volume of graft.

4. Conclusion

In summary, a novel bioartificial pancreas containing a prevascularized hydrogel scaffold and islets-laden core-shell microgels is fabricated for type 1 diabetes treatment. Specifically, GelMA/HepMA/VEGF hydrogel scaffold is formed on the surface of a silicone tube by cooling and blue light irradiation, and then implanted subcutaneously for prevascularization. In vitro transwell migration assay demonstrates that GelMA/HepMA/VEGF hydrogel can release VEGF in a sustained manner and thus recruit endothelial cells effectively. H&E staining and CD31 immunohistochemical staining of retrieved hydrogel scaffold show that GelMA/HepMA/VEGF hydrogel scaffold promotes dramatically in vivo angiogenesis. Meanwhile, islets-laden HAMA@P/C(10) core-shell microgels are prepared via droplet-based microfluidics, followed by surface photopolymerization that is controlled by photoinitiator diffusion from HAMA mono-core microgels. Protein and macrophage adsorption results suggest that P/C(10) zwitterionic hydrogel shell endows microgels with excellent anti-adhesion and mechanical strength. The live/dead staining and GSIS test confirm that the encapsulation of islets in HAMA@P/C(10) microgels doesn't affect the islets viability and insulin-secretion function. ROS and TNF-α secretion certify their low inflammation response. Finally, the as-prepared islets-laden HAMA@P/C(10) microgels are injected into the prevascularized hydrogel scaffold to form an bioartificial pancreas. This bioartificial pancreas can reverse the BGLs of diabetic mice from hyperglycemia to normoglycemia for at least 90 days, as validated by BGLs monitoring. H&E staining, CD31 immunohistochemical staining and insulin immunofluorescence staining prove the good function of bioartificial pancreas in vivo, which in our opinion is mainly ascribed to the synergistic effect among favorable microenvironment provided by HAMA core of core-shell microgel, low foreign-body reaction originated from zwitterionic hydrogel shell of core-shell microgel, and rich capillary network introduced by prevascularized GelMA/HepMA/VEGF hydrogel scaffold. We believe this bioartificial pancreas provides a new solution to type 1 diabetes treatment, and its fabrication strategy has broad potential applications in other cell therapies.

CRediT authorship contribution statement

Haofei Li: Conceptualization, Investigation, Data curation, Formal analysis, Writing – original draft. **Yulian Shang:** Conceptualization, Methodology, Investigation, Data curation, Writing – original draft. **Qi Feng:** Investigation, Methodology. **Yang Liu:** Investigation, Data curation. **Junlin Chen:** Software, Data curation. **Hua Dong:** Conceptualization, Formal analysis, Supervision, Writing – review & editing, Funding acquisition.

Declaration of competing interest

The authors declare that they have no known competing financial interests or personal relationships that could have appeared to influence the work reported in this paper.

Acknowledgements

This work was sponsored by the National Natural Science Foundation of China (Grant Nos. 51873071, 32071321) and the National Key Research and Development Program of China (2018YFC1106300).

Appendix A. Supplementary data

Supplementary data to this article can be found online at https://doi.org/10.1016/j.bioactmat.2023.04.011.

References

[1] D. Mao, M. Zhu, X. Zhang, R. Ma, X. Yang, T. Ke, L. Wang, Z. Li, D. Kong, C. Li, A macroporous heparin-releasing silk fibroin scaffold improves islet transplantation outcome by promoting islet revascularisation and survival, Acta Biomater. 59 (2017) 210.

[2] X. Wang, K. Wang, W. Zhang, M. Qiang, Y. Luo, A bilaminated decellularized scaffold for islet transplantation: structure, properties and functions in diabetic mice, Biomaterials 138 (2017) 80.

[3] K. Skrzypek, M. Nibbelink, J. Lente, M. Buitinga, M. Engelse, E. Koning, M. Karperien, A. Apeldoorn, D. Stamatialis, Pancreatic islet macroencapsulation using microwell porous membranes, Sci. Rep. 7 (2017) 9186.

[4] J. Cole, J. Florez, Genetics of diabetes mellitus and diabetes complications, Nat. Rev. Nephrol. 16 (2020) 377.
[5] M. Atkinson, G. Eisenbarth, A. Michels, Type 1 diabetes, Lancet 383 (2014) 69.
[6] R. Chang, G. Faleo, H. Russ, A. Parent, S. Elledge, D. Bernards, J. Allen, K. Villanueva, M. Hebrok, Q. Tang, T. Desai, Nanoporous immunoprotective device for stem-cell-derived β-cell replacement therapy, ACS Nano 11 (2017) 7747.
[7] T. Brusko, H. Russ, C. Stabler, Strategies for durable β cell replacement in type 1 diabetes, Science 373 (2021) 516.
[8] A. Shapiro, J. Lakey, E. Ryan, G. Korbutt, E. Toth, G. Warnock, N. Kneteman, R. Rajotte, Islet transplantation in seven patients with type 1 diabetes mellitus using a glucocorticoid-free immunosuppressive regimen, N. Engl. J. Med. 343 (2000) 230.
[9] J. Zhang, Y. Zhu, J. Song, T. Xu, J. Yang, Y. Du, L. Zhang, Rapid and long-term glycemic regulation with a balanced charged immune-evasive hydrogel in T1DM mice, Adv. Funct. Mater. 29 (2019), 1900140.
[10] Q. Yao, Z. Huang, Y. Zhai, M. Yue, L. Luo, P. Xue, Y. Han, H. Xu, L. Kou, Y. Zhao, Localized controlled release of bilirubin from β-cyclodextrin-conjugated ε-polylysine to attenuate oxidative stress and inflammation in transplanted islets, ACS Appl. Mater. Interfaces 12 (2020) 5462.
[11] S. Farah, J. Doloff, P. Müller, A. Sadraei, H. Han, K. Olafson, K. Vyas, H. Tam, J. Hollister-Lock, P. Kowalski, M. Griffin, A. Meng, M. McAvoy, A. Graham, J. McGarrigle, J. Oberholzer, G. Weir, D. Greiner, R. Langer, D. Anderson, Long-term implant fibrosis prevention in rodents and non-human primates using crystallized drug formulations, Nat. Mater. 18 (2019) 892.
[12] R. Kuwabara, S. Hu, A. Smink, G. Orive, J. Lakey, P. Vos, Applying immunomodulation to promote longevity of immunoisolated pancreatic islet grafts, Tissue Eng. B Rev. 28 (2022) 129.
[13] S. Wu, L. Wang, Y. Fang, H. Huang, X. You, J. Wu, Advances in encapsulation and delivery strategies for islet transplantation, Adv. Healthcare Mater. 10 (2021), 2100965.
[14] M. Omami, J. McGarrigle, M. Reedy, D. Isa, S. Ghani, E. Marchese, M. Bochenek, M. Longi, Y. Xing, I. Joshi, Y. Wang, J. Oberholzer, Islet microencapsulation: strategies and clinical status in diabetes, Curr. Diabetes Rep. 17 (2017) 47.
[15] T. Desai, L. Shea, Advances in islet encapsulation technologies, Nat. Rev. Drug Discov. 16 (2017) 338.
[16] Z. Samsonchi, H. Karimi, Z. Izadi, P. Baei, M. Najarasl, M. Ashtiani, J. Mohammadi, M. Moazenchi, Y. Tahamtani, H. Baharvand, E. Hajizadeh-Saffar, H. Daemi, Transplantation of islet-containing microcapsules modified with constitutional isomers of sulfated alginate in diabetic mice to mitigate fibrosis for long-term glycemic control, Chem. Eng. J. 432 (2022), 134298.
[17] T. Watanabe, T. Okitsu, F. Ozawa, S. Nagata, H. Matsunari, H. Nagashima, M. Nagaya, H. Teramae, S. Takeuchi, Millimeter-thick xenoislet-laden fibers as retrievable transplants mitigate foreign body reactions for long-term glycemic control in diabetic mice, Biomaterials 255 (2020), 120162.
[18] D. An, L. Wang, A. Ernst, A. Chiu, Y. Lu, J. Flanders, A. Datta, M. Ma, An atmosphere-breathing refillable biphasic device for cell replacement therapy, Adv. Mater. 31 (2019), 1905135.
[19] S. Chen, J. Luo, L. Shen, X. Liu, W. Wang, J. Xu, Y. Ren, Y. Ye, G. Shi, F. Cheng, L. Cheng, X. Su, L. Dai, M. Gou, H. Deng, 3D printing mini-capsule device for islet delivery to treat type 1 diabetes, ACS Appl. Mater. Interfaces 14 (2022), 23139.
[20] A. Vlahos, I. Talior-Volodarsky, S. Kinney, M. Sefton, A scalable device-less biomaterial approach for subcutaneous islet transplantation, Biomaterials 269 (2021), 120499.
[21] D. Headen, G. Aubry, H. Lu, A. García, Microfluidic-based generation of size-controlled, biofunctionalized synthetic polymer microgels for cell encapsulation, Adv. Mater. 26 (2014) 3003.
[22] T. Pham, P. Tran, C. Phung, H. Nguyen, C. Nguyen, C. Yong, J. Kim, S. Yook, J. Jeong, Surface-triggered in situ gelation for tunable conformal hydrogel coating of therapeutic cells and biomedical devices, Adv. Funct. Mater. 31 (2021), 2010169.
[23] J. Weaver, D. Headen, M. Coronel, M. Hunckler, H. Shirwan, A. García, Synthetic poly(ethylene glycol)-based microfluidic islet encapsulation reduces graft volume for delivery to highly vascularized and retrievable transplant site, Am. J. Transplant. 19 (2019) 1315.
[24] M. Kim, H. Kim, Y. Lee, S. Lee, S. Kim, U. Lee, S. Jung, C. Park, J. Hong, J. Doh, D. Lee, B. Kim, N. Hwang, Novel enzymatic cross-linking-based hydrogel nanofilm caging system on pancreatic β cell spheroid for long-term blood glucose regulation, Sci. Adv. 7 (2021), eabf7832.
[25] Z. Izadi, E. Hajizadeh-Saffar, J. Hadjati, M. Habibi-Anbouhi, M. Ghanian, H. Sadeghi-Abandansari, M. Ashtiani, Z. Samsonchi, M. Raoufi, M. Moazenchi, M. Izadi, A. Nejad, H. Namdari, Y. Tahamtani, S. Ostad, H. Akbari-Javar, H. Baharvand, Tolerance induction by surface immobilization of Jagged-1 for immunoprotection of pancreatic islets, Biomaterials 182 (2018) 191.
[26] Ryo Kogawa, Kentaro Nakamura, Yusuke Mochizuki, A new islet transplantation method combining mesenchymal stem cells with recombinant peptide pieces, microencapsulated islets, and mesh bags, Biomedicines 8 (2020) 299.
[27] O. Korsgren, T. Lundgren, M. Felldin, A. Foss, B. Isaksson, J. Permert, N. Persson, E. Rafael, M. Rydén, K. Salmela, A. Tibell, G. Tufveson, B. Nilsson, Optimising islet engraftment is critical for successful clinical islet transplantation, Diabetol 51 (2008) 227.
[28] A. Espona-Noguera, J. Ciriza, A. Cañibano-Hernández, G. Orive, R. Hernández, L. Burgo, J. Pedraz, Review of advanced hydrogel-based cell encapsulation systems for insulin delivery in type 1 diabetes mellitus, Pharmaceutics 11 (2019) 597.
[29] A. Smink, M. Faas, P. Vos, Toward engineering a novel transplantation site for human pancreatic islets, Diabetes 62 (2013) 1357.
[30] A. Pepper, B. Gala-Lopez, R. Pawlick, S. Merani, T. Kin, A. Shapiro, A prevascularized subcutaneous device-less site for islet and cellular transplantation, Nat. Biotechnol. 33 (2015) 518.
[31] A. Shapiro, M. Pokrywczynska, C. Ricordi, Clinical pancreatic islet transplantation, Nat. Rev. Endocrinol. 13 (2017) 268.
[32] A. Pepper, R. Pawlick, B. Gala-Lopez, A. MacGillivary, D. Mazzuca, D. White, P. Toleikis, A. Shapiro, Diabetes is reversed in a murine model by marginal mass syngeneic islet transplantation using a subcutaneous cell pouch device, Transplantation 99 (2015) 2294.
[33] F. Cayabyab, L. Nih, E. Yoshihara, Advances in pancreatic islet transplantation sites for the treatment of diabetes, Front. Endocrinol. 12 (2021), 732431.
[34] A. Mridha, T. Dargaville, P. Dalton, L. Carroll, M. Morris, V. Vaithilingam, B. Tuch, Prevascularized retrievable hybrid implant to enhance function of subcutaneous encapsulated islets, Tissue Eng. Part A 28 (2022) 212.
[35] W. Song, A. Chiu, L. Wang, R. Schwartz, B. Li, N. Bouklas, D. Bowers, D. An, S. Cheong, J. Flanders, Y. Pardo, Q. Liu, X. Wang, V. Lee, G. Dai, M. Ma, Engineering transferrable microvascular meshes for subcutaneous islet transplantation, Nat. Commun. 10 (2019) 4602.
[36] A. Vlahos, N. Cober, M. Sefton, Modular tissue engineering for the vascularization of subcutaneously transplanted pancreatic islets, Proc. Natl. Acad. Sci. U.S.A. 114 (2017) 9337.
[37] Y. Sato, H. Endo, H. Okuyama, T. Takeda, H. Iwahashi, A. Imagawa, K. Yamagata, I. Shimomura, M. Inoue, Cellular hypoxia of pancreatic β-cells due to high levels of oxygen consumption for insulin secretion in vitro, J. Biol. Chem. 286 (2011), 12524.
[38] A. Smink, S. Li, D. Hertsig, B. Haan, L. Schwab, A. Apeldoorn, E. Koning, M. Faas, J. Lakey, P. Vos, The efficacy of a prevascularized, retrievable poly(D,L,-lactide-co-ε-caprolactone) subcutaneous scaffold as transplantation site for pancreatic islets, Transplantation 101 (2017) e112.
[39] N. Kasoju, A. Pátíková, E. Wawrzynska, A. Vojtíšková, T. Sedlačík, M. Kumorek, O. Pop-Georgievski, E. Sticová, J. KříŽ, D. Kubies, Bioengineering a pre-vascularized pouch for subsequent islet transplantation using VEGF-loaded polylactide capsules, Biomater. Sci. 8 (2020) 631.
[40] D. Bowers, W. Song, L. Wang, M. Ma, Engineering the vasculature for islet transplantation, Acta Biomater. 95 (2019) 131.
[41] J. Zhou, Y. Lin, L. Wang, L. Zhou, B. Yu, X. Zou, Z. Luo, H. Hu, Poly(carboxybetaine methacrylate) grafted on PVA hydrogel via a novel surface modification method under near-infrared light for enhancement of antifouling properties, Colloids Surf. A Physicochem. Eng. Aspects 617 (2021), 126369.
[42] T. Ma, X. Gao, H. Dong, H. He, X. Cao, High-throughput generation of hyaluronic acid microgels via microfluidics-assisted enzymatic crosslinking and/or Diels-Alder click chemistry for cell encapsulation and delivery, Appl. Mater. Today 9 (2017) 49.
[43] H. Ye, J. Cheng, K. Yu, In situ reduction of silver nanoparticles by gelatin to obtain porous silver nanoparticle/chitosan composites with enhanced antimicrobial and wound-healing activity, Int. J. Biol. Macromol. 121 (2019) 633.
[44] T. Yao, H. Chen, R. Wang, R. Rivero, F. Wang, L. Kessels, S. Agten, T. Hackeng, T. Wolfs, D. Fan, M. Baker, L. Moroni, Thiol-ene conjugation of a VEGF peptide to electrospun scaffolds for potential applications in angiogenesis, Bioact. Mater. 20 (2023) 306.
[45] K. Wang, X. Chen, Y. Pan, Y. Cui, X. Zhou, D. Kong, Z. Qiang, Enhanced vascularization in hybrid PCL/gelatin fibrous scaffolds with sustained release of VEGF, BioMed Res. Int. 2015 (2015), 865076.
[46] F. Gao, Z. Xu, Q. Liang, H. Li, L. Peng, M. Wu, X. Zhao, X. Cui, C. Ruan, W. Liu, Osteochondral regeneration with 3D-printed biodegradable high-strength supramolecular polymer reinforced-gelatin hydrogel scaffolds, Adv. Sci. 6 (2019), 1900867.
[47] Z. Luo, W. Sun, J. Fang, K. Lee, S. Li, Z. Gu, M. Dokmeci, A. Khademhosseini, Biodegradable gelatin methacryloyl microneedles for transdermal drug delivery, Adv. Healthcare Mater. 8 (2019), 1801054.
[48] C. Onofrillo, S. Duchi, S. Francis, C. O'Connell, L. Aguilar, S. Doyle, Z. Yue, G. Wallace, P. Choong, C. Bella, FLASH: fluorescently LAbelled Sensitive Hydrogel to monitor bioscaffolds degradation during neocartilage generation, Biomaterials 264 (2021), 120383.
[49] H. Wen, J. Li, G. Payne, Q. Feng, M. Liang, J. Chen, H. Dong, X. Cao, Hierarchical patterning via dynamic sacrificial printing of stimuli-responsive hydrogels, Biofabrication 12 (2020), 035007.
[50] H. Su, Q. Li, D. Li, H. Li, Q. Feng, X. Cao, H. Dong, A versatile strategy to construct free-standing multi-furcated vessels and a complicated vascular network in heterogeneous porous scaffolds via combination of 3D printing and stimuli-responsive hydrogels, Mater. Horiz. 9 (2022) 2393.
[51] F. Kocak, M. Yar, I. Rehman, Hydroxyapatite-integrated, heparin- and glycerol-functionalized chitosan-based injectable hydrogels with improved mechanical and proangiogenic performance, Int. J. Mol. Sci. 23 (2022) 5370.
[52] N. Zhao, A. Suzuki, X. Zhang, P. Shi, L. Abune, J. Coyne, H. Jia, N. Xiong, G. Zhang, Y. Wang, Dual aptamer-functionalized in situ injectable fibrin hydrogel for promotion of angiogenesis via codelivery of vascular endothelial growth factor and platelet-derived growth factor-BB, ACS Appl. Mater. Interfaces 11 (2019), 18123.
[53] R. Chen, E. Silva, W. Yuen, A. Brock, C. Fischbach, A. Lin, R. Guldberg, D. Mooney, Integrated approach to designing growth factor delivery systems, Faseb. J. 21 (2007) 3896.
[54] W. Zhu, X. Qu, J. Zhu, X. Ma, S. Patel, J. Liu, P. Wang, C. Lai, M. Gou, Y. Xu, K. Zhang, S. Chen, Direct 3D bioprinting of prevascularized tissue constructs with complex microarchitecture, Biomaterials 124 (2017) 106.
[55] D. Lan, Y. Shang, H. Su, M. Liang, Y. Liu, H. Li, Q. Feng, X. Cao, H. Dong, Facile fabrication of hollow hydrogel microfiber via 3D printing-assisted microfluidics

and its application as a biomimetic blood capillary, ACS Biomater. Sci. Eng. 7 (2021) 4971.
[56] F. Lei, M. Liang, Y. Liu, H. Huang, H. Li, H. Dong, Multi-compartment organ-on-a-chip based on electrospun nanofiber membrane as in vitro jaundice disease model, Adv. Fiber Mater. 3 (2021) 383.
[57] Q. Feng, Q. Li, H. Wen, J. Chen, M. Liang, H. Huang, D. Lan, H. Dong, X. Cao, Injection and self-assembly of bioinspired stem cell-laden gelatin/hyaluronic acid hybrid microgels promote cartilage repair in vivo, Adv. Funct. Mater. 29 (2019), 1906690.
[58] Q. Feng, D. Li, Q. Li, S. Li, H. Huang, H. Li, H. Dong, X. Cao, Dynamic nanocomposite microgel assembly with microporosity, injectability, tissue-adhesion, and sustained drug release promotes articular cartilage repair and regeneration, Adv. Healthcare Mater. 11 (2022), 2102395.
[59] Q. Feng, H. Gao, H. Wen, H. Huang, Q. Li, M. Liang, Y. Liu, H. Dong, X. Cao, Engineering the cellular mechanical microenvironment to regulate stem cell chondrogenesis: insights from a microgel model, Acta Biomater. 113 (2020) 393.
[60] Q. Feng, D. Li, Q. Li, H. Li, Z. Wang, S. Zhu, Z. Lin, X. Cao, H. Dong, Assembling microgels via dynamic cross-linking reaction improves printability, microporosity, tissue-adhesion, and self-healing of microgel bioink for extrusion bioprinting, ACS Appl. Mater. Interfaces 14 (2022), 15653.
[61] Y. Liu, X. Zhang, T. Wu, B. Liu, J. Yang, W. Liu, Chinese herb-crosslinked hydrogel bearing rBMSCs-laden polyzwitterion microgels: self-adaptive manipulation of micromilieu and stemness maintenance for restoring infarcted myocardium, Nano Today 41 (2021), 101306.
[62] Z. Xiao, T. Wei, R. Ge, Q. Li, B. Liu, Z. Ji, L. Chen, J. Zhu, J. Shen, Z. Liu, Y. Huang, Y. Yang, Q. Chen, Microfluidic production of zwitterion coating microcapsules with low foreign body reactions for improved islet transplantation, Small 18 (2022), 2202596.
[63] X. Liang, L. Xie, Q. Zhang, G. Wang, S. Zhang, M. Jiang, R. Zhang, T. Yang, X. Hu, Z. Yang, W. Tian, Gelatin methacryloyl-alginate core-shell microcapsules as efficient delivery platforms for prevascularized microtissues in endodontic regeneration, Acta Biomater. 144 (2022) 242.
[64] Y. Chandorkar, K. Ravikumar, B. Basu, The foreign body response demystified, ACS Biomater. Sci. Eng. 5 (2019) 19.
[65] Y. Song, L. Li, W. Zhao, Y. Qian, L. Dong, Y. Fang, L. Yang, Y. Fan, Surface modification of electrospun fibers with mechano-growth factor for mitigating the foreign-body reaction, Bioact. Mater. 6 (2021) 2983.
[66] Y. Lin, L. Wang, J. Zhou, L. Ye, H. Hu, Z. Luo, L. Zhou, Surface modification of PVA hydrogel membranes with carboxybetaine methacrylate via PET-RAFT for anti-fouling, Polymer 162 (2019) 80.
[67] B. He, J. Yang, Y. Liu, X. Xie, H. Hao, X. Xing, W. Liu, An in situ-forming polyzwitterion hydrogel: towards vitreous substitute application, Bioact. Mater. 6 (2021) 3085.
[68] H. Huang, Y. Shang, H. Li, Q. Feng, Y. Liu, J. Chen, H. Dong, Co-transplantation of islets-laden microgels and biodegradable O_2-generating microspheres for diabetes treatment, ACS Appl. Mater. Interfaces 14 (2022), 38448.
[69] Y. Jun, J. Lee, S. Choi, J. Yang, M. Sander, S. Chung, S. Lee, In vivo-mimicking microfluidic perfusion culture of pancreatic islet spheroids, Sci. Adv. 5 (2019) eaax4520.
[70] S. Song, R. Yeung, J. Park, A. Posselt, T. Desai, Q. Tang, S. Roy, Glucose-stimulated insulin response of silicon nanopore-immunoprotected islets under convective transport, ACS Biomater. Sci. Eng. 3 (2017) 1051.
[71] Y. Wang, J. Liu, C. Liu, A. Naji, D. Stoffers, MicroRNA-7 regulates the mTOR pathway and proliferation in adult pancreatic β-cells, Diabetes 62 (2013) 887.
[72] H. Wang, B. Wei, H. He, X. Huang, J. Sheng, X. Chen, L. Wang, R. Tan, J. Li, J. Liu, S. Yang, R. Ma, H. Lan, Smad3 deficiency improves islet-based therapy for diabetes and diabetic kidney injury by promoting β cell proliferation via the E2F3-dependent mechanism, Theranostics 12 (2022) 379.
[73] D. Zhang, Q. Chen, C. Shi, M. Chen, K. Ma, J. Wan, R. Liu, Dealing with the foreign-body response to implanted biomaterials: strategies and applications of new materials, Adv. Funct. Mater. 31 (2021), 2007226.
[74] M. Brereton, M. Iberl, K. Shimomura, Q. Zhang, A. Adriaenssens, P. Proks, I. Spiliotis, W. Dace, K. Mattis, R. Ramracheya, F. Gribble, F. Reimann, A. Clark, P. Rorsman, F. Ashcroft, Reversible changes in pancreatic islet structure and function produced by elevated blood glucose, Nat. Commun. 5 (2014) 4639.
[75] Z. Wang, N. York, C. Nichols, M. Remedi, Pancreatic β cell dedifferentiation in diabetes and redifferentiation following insulin therapy, Cell Metabol. 19 (2014) 872.
[76] A. Williams, W. Chau, M. Callaway, C. Dayan, Magnetic resonance imaging: a reliable method for measuring pancreatic volume in type 1 diabetes, Diabet. Med. 24 (2007) 35.